Functionality of potato virus Y coat protein in cell-to-cell movement is defined by flexibility of its N terminal region

Anže Vozelj[1,2*], Tjaša Mahkovec Povalej[1], Katja Stare[1], Magda Tušek Žnidarič[1], Katarina Bačnik[1], Valentina Levak[1,2], Ion Gutiérrez-Aguirre[1], Marjetka Podobnik[3], Kristina Gruden[1], Anna Coll[1]†, Tjaša Lukan[1]†*

[1]Department of Biotechnology and Systems Biology, National Institute of Biology, Večna pot 121, 1000 Ljubljana, Slovenia

[2]Jožef Stefan International Postgraduate School, Jamova cesta 39, 1000 Ljubljana, Slovenia

[3]Department of Molecular Biology and Nanobiotechnology, National Institute of Chemistry, Hajdrihova 19, 1001 Ljubljana, Slovenia

* Corresponding authors.

Email: anze.vozelj@nib.si, tjasa.lukan@nib.si

† shared last authorship

Abstract

Potato virus Y (PVY) is one of the top ten economically most important plant viruses and responsible for major yield losses. We previously suggested the involvement of the N terminal region of potato virus Y coat protein (CP) in PVY spread. By constructing different N terminal deletion mutants of PVY N605 strain, we here show that deletions of 40 or more amino acid residues from the N terminal region of the CP resulted in the PVY multiplication limited to primary infected cells in *Nicotiana clevelandii* plants. Deletion of 26 residues profoundly impaired PVY cell-to-cell movement and prevented systemic PVY spread, while deletions of 19-23 residues allowed delayed systemic PVY spread. Introduced point mutations in the identified region prevent (S21G) or delay (G20P) PVY movement. In summary, this work shows the significance of the N-terminus flexibility for movement of the PVY.

Keywords: potato virus Y, potato (*Solanum tuberosum*), coat protein (CP), viral movement, point mutations

Introduction

Plants undergo constant exposure to various pathogens and pests, with viruses being the most severe amongst them. Potato virus Y (PVY) is classified amongst the top ten economically most important plant viruses infecting solanaceous crops including potato, tomato, tobacco and pepper (Scholthof et. al., 2011). PVY is the causal agent of potato tuber necrosis ringspot disease (Quenouille et. al., 2013), a devastating disease that negatively impacts potato tuber quality and yield (Ivanov et. al., 2014).

PVY belongs to *Potyvirus* genus. Its genome consists of 9,7-kb positive sense single stranded RNA (+ ssRNA) encoding for single open reading frame (ORF) that is translated into 350 kDa long polyprotein which is cleaved into 10 mature proteins (Ivanov et. al., 2014). Furthermore, PVY genome contains an additional ORF *pipo*, embedded within the P3 cistron of the polyprotein, that via transcriptional slippage results in production of the so called “Pretty interesting potyviridae ORF” (P3N-PIPO) protein (Chung et. al., 2008).

The majority of potyviral proteins are multifunctional and they altogether contribute to the establishment of successful viral infection, that encompasses multiple steps including transmission by aphids, penetration of viral particles into the cell, virion disassembly, translation, replication, suppression of host defense mechanisms, virion assembly and virus movement from the primary infected cells to neighboring cells and systemic spread (Yang et. al., 2021).

Viral movement is facilitated through plasmodesmata, plant specific structures connecting two adjacent cells that serve as gateways for cell-to-cell movement and contribute to the establishment of systemic infection (Benitez-Alfonso et. al., 2010; Folimonova and Tilsner, 2018; Reagan and Burch-Smith, 2020; Revers and García, 2015). At least four potyviral proteins, coat protein (CP), cylindrical inclusion protein (CI), P3N-PIPO and the second 6 kDa protein (6K2) protein are essential for cell-to-cell movement of potyviruses (Xue et. al., 2023). P3N-PIPO is localized in the plasmodesmata and directs CI to form conical structures that are crucial for assistance of potyviral intercellular movement through plasmodesmata, which was shown for turnip mosaic virus (TuMV)

64 in *Nicotiana benthamiana* (Wei et. al., 2010). Accumulation of CP in plasmodesmata during
65 infection is also crucial since together with the potyviral Helper-Component Proteinase (HCPro)
66 increases the size exclusion limit (SEL) of plasmodesmata, which was determined by microinjection
67 studies for bean common mosaic necrosis potyvirus (BCMNV) in *N. benthamiana* (Rojas et. al.,
68 1997). Systemic infection encompasses viral movement through phloem and less often through
69 xylem to reach and infect plant distant tissues (Navarro et. al., 2019; Mäkinen and Hafren, 2014).
70 However, before reaching vasculature, plant viruses need to cross various cellular barriers
71 including bundle sheath, vascular parenchyma and companion cells, to reach sieve elements,
72 through which they are transported to distant tissues (Navarro et. al., 2019). The invasion of distant
73 tissues requires unloading from sieve elements into companion cells and cell-to-cell movement into
74 bundle sheath and mesophyll cells (Navarro et. al., 2019). Despite PVY being one of the most
75 extensively studied potyviruses on molecular scale, information about crucial factors governing cell-
76 to-cell as well as systemic spread are scarce (Yang et. al., 2021; Xue et. al., 2023).

77 The cryo-EM structures of some potyviruses including PVY, watermelon mosaic virus (WMV) and
78 TuMV virions have been determined and offered a detailed insight into the conserved helical
79 arrangement of CPs assembled around viral ssRNA as well as the conserved three dimensional
80 structure of CP among them (Kežar et. al., 2019; Zamora et. al., 2017; Cuesta et. al., 2019). CP is
81 the only potyviral structural protein and more than 2000 copies of CP encapsidate the viral ssRNA
82 molecule to form potyviral virions (Yang et. al., 2021; Revers et. al., 2015). Individual CP is built of
83 three distinct regions. The N terminal region with residues up to Val44 in PVY, which are exposed
84 at the outer surface of the virus, are flexible and thus its 3D structure was not determined. The rest
85 of N terminal region, from Val44 to Gln76, is structured. It has an extended structure with one short
86 alpha helix in the middle (Kežar et. al., 2019). The central core has a globular shape. The C terminal
87 region is in the lumen of the virus and its extended structure is supported by the viral ssRNA scaffold
88 (Kežar et. al., 2019). Beyond its primary role in viral encapsidation, the CP is indispensable for
89 aphid transmission, potyviral RNA amplification and cell-to-cell movement (Revers and García,
90 2015; Rojas et. al., 1997; Dai et. al., 2020). Functional studies of the CP protein indicate crucial

91 roles of its N and C terminal regions and the core region in potyvirus infectivity. In the case of PVY,
92 the absence of the flexible CP N terminal region hinders the formation of filaments and cell-to-cell
93 viral movement (Kežar et. al., 2019). For soybean mosaic virus (SMV), the CP C terminal region is
94 involved in CP intersubunit interactions, viral cell-to-cell and long distance movement and virion
95 assembly (Seo et. al., 2013). In potato virus A (PVA), phosphorylation of Thr243 residue on CP C
96 terminal region is crucial for PVA replication *in planta* (Lõhmus et. al., 2017). These results and
97 results of several other studies suggest that different CP regions are important for cell-to-cell
98 movement of potyviruses (Dolja et. al., 1994; Arazi et. al., 2001; Kimalov et. al., 2004; Tatineni et.
99 al., 2014; Tatineni and French, 2014; Tatineni et. al., 2017). It is not known yet in what structural
100 shape are the viruses propagated through the plant, as assembled virions or viral ribonucleoprotein
101 (RNP) complexes associated with CP (Navarro et. al., 2019; Mäkinen et. al., 2014).

102 The so far generated evidence-based knowledge differs from one potyvirus to another, and thus,
103 more research is needed to comprehensively elucidate these complex processes, particularly for
104 those economically relevant potyviruses such as PVY. By constructing different PVY N terminal
105 deletion mutants, we identified the regions of the CP that are important for efficient PVY cell-to-cell
106 movement.

107

108 **Results**
109
110 **Deletion of 40 or more amino acid residues from the PVY CP N terminal region affects cell-**
111 **to-cell movement, but does not prevent replication**

112 Previously we showed that PVY with deleted 50 N terminal amino acid residues was still able to
113 replicate but based on the low and spatially limited levels of RNA accumulation, we suggested that
114 N terminal region is required for cell-to-cell movement (Kežar et. al., 2019). To confirm this
115 hypothesis, we here constructed two GFP-tagged PVY (PVY N605-GFP) mutants lacking either 40
116 or 50 amino acid residues at the CP N terminal region (hereafter ΔN50-CP and ΔN40-CP). In all
117 constructed mutants GFP was inserted between NIb and CP coding sequence, flanked by protease
118 recognition sites, allowing GFP excision from the polyprotein after translation (Lukan et. al., 2023).
119 We followed the spread of ΔN50-CP and ΔN40-CP with confocal microscopy upon bombardment
120 of *Nicotiana clevelandii* leaves (Fig. 1B). Neither mutant was able to move cell-to-cell, remaining
121 limited to bombarded cells (Fig. 1B). We detected viral RNA replication of both mutants in the
122 bombarded leaves, albeit at significantly lower levels in comparison to the non-mutated clone
123 (hereafter WT-CP) (Fig. S1, data S1 and S2). Despite the lower RNA levels observed in leaves
124 bombarded with constructed mutants, confocal microscopy image analysis showed that the
125 accumulation of GFP in individual infected cells was the same in WT and ΔN40-CP mutant,
126 confirming unhindered replication (Table S2). These findings corroborate our previous results
127 showing that N terminal region CP truncations still allow viral replication (Kežar et. al., 2019) and
128 further show that the absence of either 50 or 40 N-terminal residues abolish cell-to-cell viral
129 movement.

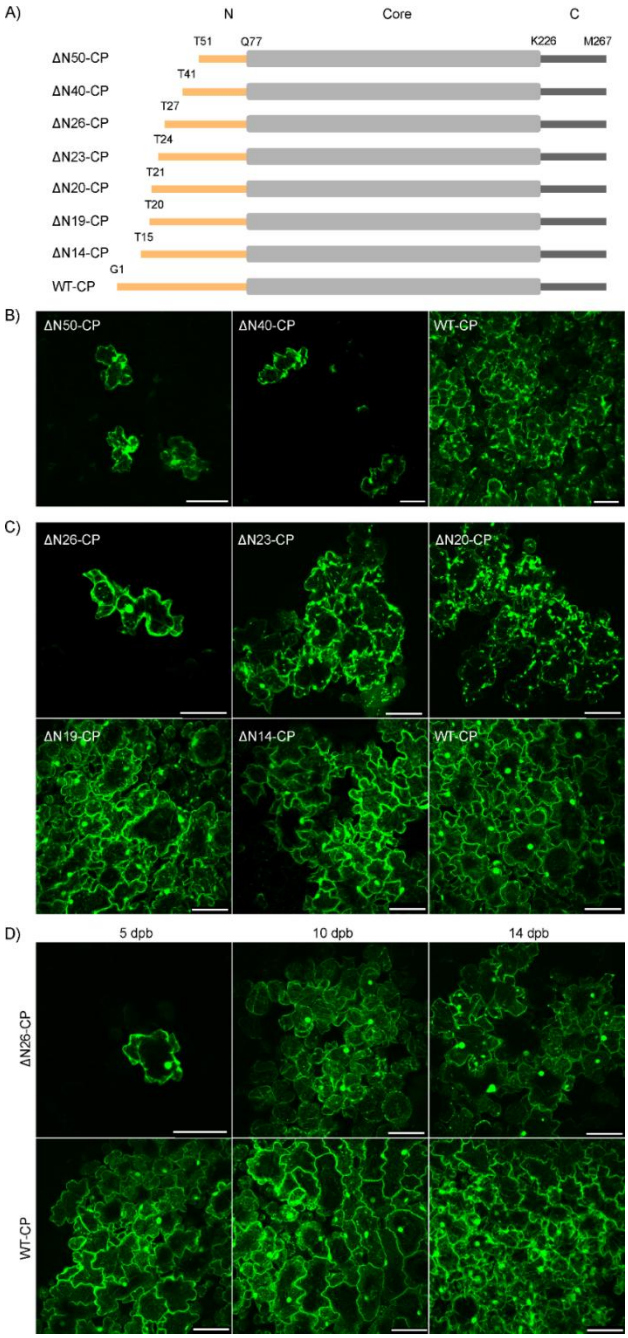

Figure 1. Amino acid deletions at PVY CP N terminal region influence viral cell-to-cell movement. **(A)** Schematic representation of constructed mutants with deletions on PVY CP N terminal region (N-terminal region, orange; core region, grey; C-terminal region, dark grey) with labeled amino acids. **(B)** Confocal microscopy images showing viral replication is limited to single cells when 50 (ΔN50-CP) or 40 (ΔN40-CP) amino acid residues were deleted at CP N terminal region, while non-mutated clone (WT-CP) shows cell-to-cell spread 10-12 days post bombardment (dpb). Scale bar: 100 μm. **(C)** 5 dpb viral replication is limited to

138 single cells in ΔN26-CP mutant, while cell-to-cell virus spread was observed for CP deletion mutants ΔN23-
139 CP, ΔN20-CP, ΔN19-CP, ΔN14-CP. Scale bar: 100 µm. **(D)** ΔN26-CP cell-to cell-spread was observed at later
140 time points (10 and 14 dpb). Scale bar: 100 µm.

141 **The deletions of 19-26 amino acid residues of the PVY CP N terminal region are influencing**
142 **dynamics of viral cell-to-cell spread**

143 To further assess which region of CP N terminal is crucial for cell-to-cell virus spread, we
144 constructed GFP-tagged mutants lacking 26, 23, 20, 19 and 14 amino acid residues at the CP N
145 terminal region (Fig. 1A) and followed their localization under confocal microscope at different time
146 points after virus inoculation (Fig. 1, C and D, data S2 and table S1). Mutants lacking 26 (ΔN26 -
147 CP) and 23 (ΔN23 -CP) residues on CP N terminal region had the first non deleted amino acid
148 replaced with glycine (G) during the mutagenesis.

149 At 5 dpb, ΔN14-CP and ΔN19-CP mutants did not show any differences in cell-to-cell spread
150 compared to WT-CP, while a lower spread level was noticed for ΔN20-CP and ΔN23-CP (Fig. 1C).
151 The most pronounced difference in comparison to other mutants and to WT-CP was observed in
152 the case of ΔN26-CP mutant, which remained confined to single cells at 5 dpb (Fig. 1, C and D).
153 However, at later time points (10 and 14 dpb), in approximately half of the infected plants, we also
154 observed cell-to-cell viral movement, although substantially delayed compared to WT-CP (Fig. 1D
155 and table S1). Also, the measured viral RNA load for ΔN26-CP mutant was significantly lower than
156 that of WT-CP at all 5 dpb, 10 and 14 dpb (fig. S2 and data S1).

157 Whole plant imaging was conducted to more precisely examine the dynamics of cell-to-cell virus
158 spread of WT-CP, ΔN23-CP, ΔN19-CP and ΔN14-CP through time on inoculated *N. clevelandii*
159 leaves (Fig. 2A). As expected, the results revealed statistically significant differences in the viral
160 multiplication area between N23-CP and WT-CP, and ΔN19-CP compared to WT-CP (Fig. 2, B and
161 C and data S3 and S4). A similar though less evident trend was observed in the case of ΔN14-CP
162 compared to WT-CP, which was not statistically significant (Fig.2 C and data S4).

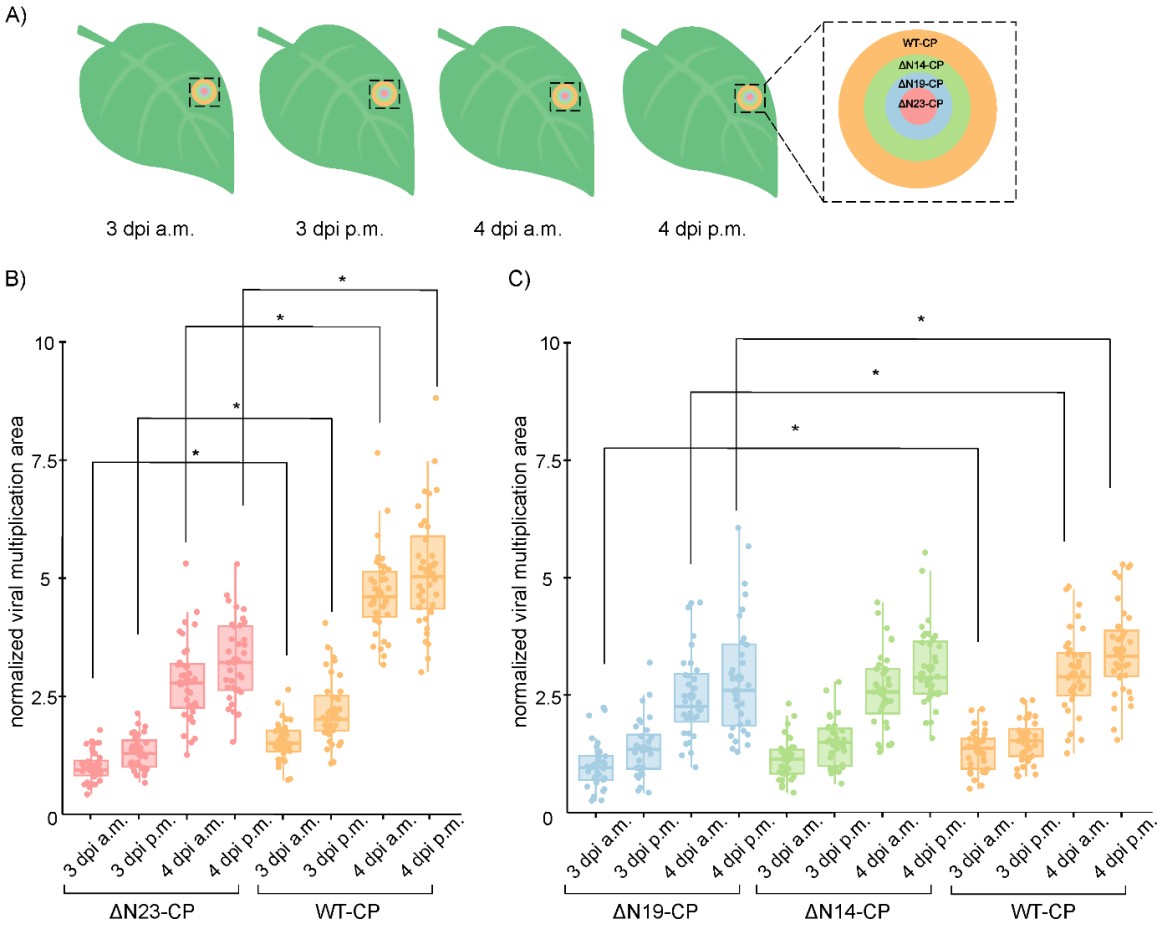

Figure 2. Precise analysis of the viral multiplication areas revealed a hampered cell-to-cell virus spread in ΔN19-CP and ΔN23-CP mutants. (A) The scheme of the viral multiplication area at different time points for all mutants compared with WT-CP. The area was followed by more precise analysis using whole plant imaging system for examining cell-to-cell virus spread of ΔN23-CP, ΔN19-CP, ΔN14-CP and WT-CP in four timepoints including 3 days post inoculation (dpi) in the morning (a.m), 3 dpi in the afternoon (p.m), 4 dpi a.m. and 4 dpi p.m. Note that the viral multiplication area was the largest after infection with WT-CP and decreased in the latter order ΔN14-CP, ΔN19-CP and ΔN23-CP. **(B and C)** Normalized viral multiplication area. After inoculating leaves with WT-CP or mutants, plants were imaged with whole plant imaging system. Images of three selected viral multiplication areas per leaf per plant were taken at four time points. Differences were statistically evaluated using Welch's t test. Results are presented as boxplots with dots representing normalized viral multiplication areas (data S3 and S4) for ΔN23-CP-CP, WT-CP **(B)** and ΔN19-CP, ΔN14-CP, WT-CP **(C)**. Statistically significant differences ($p < 0.05$) are denoted with an asterisk (*). Vertical lines present all points except outliers. Raw and normalized data, number of plants and statistics are specified in Data S3

177 and S4. The same trend was observed in a replicate experiment (Fig. S3 and data S5). For comparison
178 between two independent experiments, data measured for mutant viruses were normalized to median of
179 values obtained for WT virus (data S6).

180 These results show that the dynamics of viral cell-to-cell spread is dependent on the length of the
181 CP N terminal region (Fig. 1 and data S2). More precisely, as the number of CP N terminal region
182 deleted amino acid residues increases, cell-to-cell movement speed is decreased (Fig. 2, B and C
183 and data S3, S4 and S6). We conclude that amino acids in the region 19-26 on CP N terminal
184 region are essential for an optimal PVY cell-to-cell movement.

185 **Systemic viral spread dynamics is affected by the cell-to-cell movement**

186 Since viral cell-to-cell spread is prerequisite for systemic viral spread, we further tested if the
187 observed delay in cell-to-cell viral spread of mutants (Figs. 1, C and 2, B and C) affects the systemic
188 viral spread. In contrast to the systemic spread of WT-CP, which is detectable already at 7 dpb, the
189 spread of ΔN23-CP, ΔN19-CP and ΔN14-CP mutants to systemic leaves occurs with a delay (Fig.
190 3A). If compared to WT-CP, ΔN14-CP was observed in systemic tissue with 1 day delay (8 dpb),
191 ΔN19-CP with 2 days delay (9 dpb) and ΔN23-CP with approximately 3 weeks delay (25 dpb) (Fig.
192 3A). The mutant ΔN26-CP did not reach systemic leaves even at the highest tested dpb (Fig. S4).

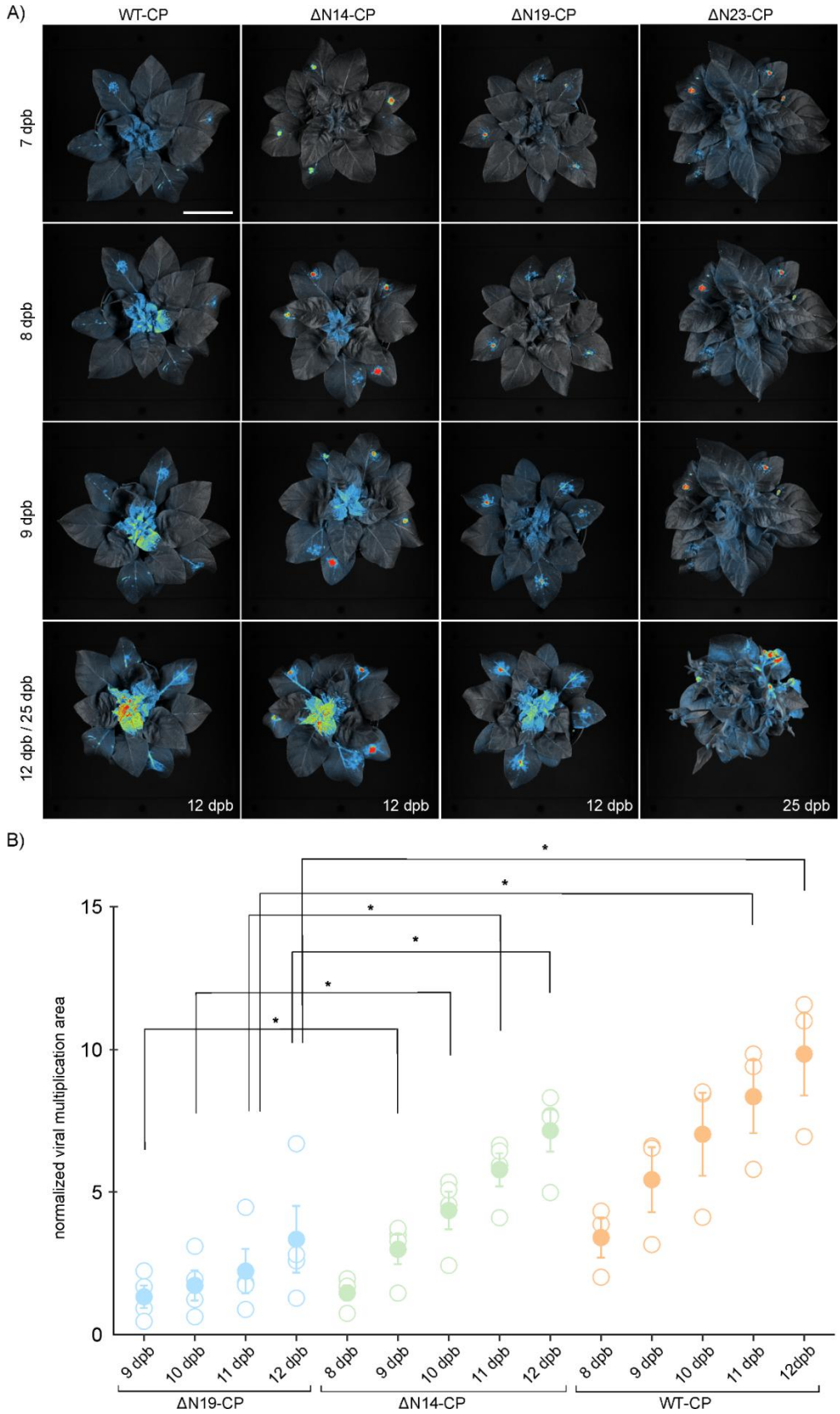
A)
WT-CP
ΔN14-CP
ΔN19-CP
ΔN23-CP
7 dpb
8 dpb
9 dpb
12 dpb / 25 dpb
12 dpb
12 dpb
12 dpb
25 dpb
B)
normalized viral multiplication area
15
10
5
0
9 dpb
10 dpb
11 dpb
12 dpb
8 dpb
9 dpb
10 dpb
11 dpb
12 dpb
8 dpb
9 dpb
10 dpb
11 dpb
12dpb
ΔN19-CP
ΔN14-CP
WT-CP

194 **Figure 3. Systemic viral spread of mutants is delayed similarly as cell-to-cell movement. (A)** Spatio-
195 temporal PVY distribution in *N. clevelandii* systemic tissue. Viral multiplication area was followed 7-12 and
196 25 days post bombardment (dpb), by using whole plant imaging system. Scale bar: 5 cm. **(B)** Quantification
197 of viral multiplication area in ROI in the *N. clevelandii* systemic tissue in total count per mutant in five
198 selected timepoints including 8-12 dpb. Since ΔN19-CP did not spread systemically at 8 dpi, normalized
199 viral multiplication area is not shown. Mean (represented with filled dot) and standard error are shown.
200 Individual measurements are shown as empty dots, representing normalized viral multiplication area.
201 Differences were statistically evaluated using Welch`s t test. Statistically significant differences ($p < 0.05$) are
202 marked with asterisk. Raw and normalized data, number of plants and statistics are specified in data S7.
203 Since ΔN26-CP is not capable of spreading systemically, it was not included in the analysis. Also ΔN23-CP
204 had such a delayed spread that it was not possible to do a quantification of viral multiplication area at 8 to 12
205 dpb (Fig. 3A).

206 Quantitative analysis of viral multiplication signal in systemic tissue confirmed that WT-CP achieved
207 the largest multiplication area, followed by ΔN14-CP and lastly ΔN19-CP in all observed time points
208 (Fig. 3 and data S7). When comparing ΔN14-CP and WT-CP, we observed a trend of slower spread
209 in case of ΔN14-CP, albeit not statistically significant (Fig. 3B and data S7). ΔN23-CP was not
210 included in the comparison, due to the considerable delay in the systemic spread exhibited by this
211 mutant (Fig. 3A), which made it difficult to measure the viral multiplication area. In conclusion,
212 systemic viral spread is abolished for ΔN26-CP, and decreasingly hampered in case of ΔN23-CP,
213 ΔN19-CP, while ΔN14-CP mutant is able to move similarly as WT-CP, albeit with a short delay.

214 **Change of flexibility in N-terminal region affects cell-to-cell viral movement**

215 To pinpoint amino acids important for cell-to-cell virus movement, we generated point mutations in
216 the part of CP N terminal region that was previously observed as being important for viral
217 movement. We point mutated charged residues Asp14, Glu18, potential phosphorylation site at
218 Ser21 and 3D structure breakers Gly20 and Pro24. All, except Pro24, are highly conserved across
219 sequenced PVY strains. At position 24, 50% of PVY strains carries Pro and the others Ser (Fig S9).
220 Selected residues were changed to Ala (D14A, E18A, P24A), except for Ser21 where the sequence

221 coding for Ala and Thr substitution was unstable in *E. coli*, thus we mutated it to Gly (S21G) and

222 for Gly20, where we intentionally introduced Pro (G20P) to affect the fold of N terminal region (Fig.

223 4A).

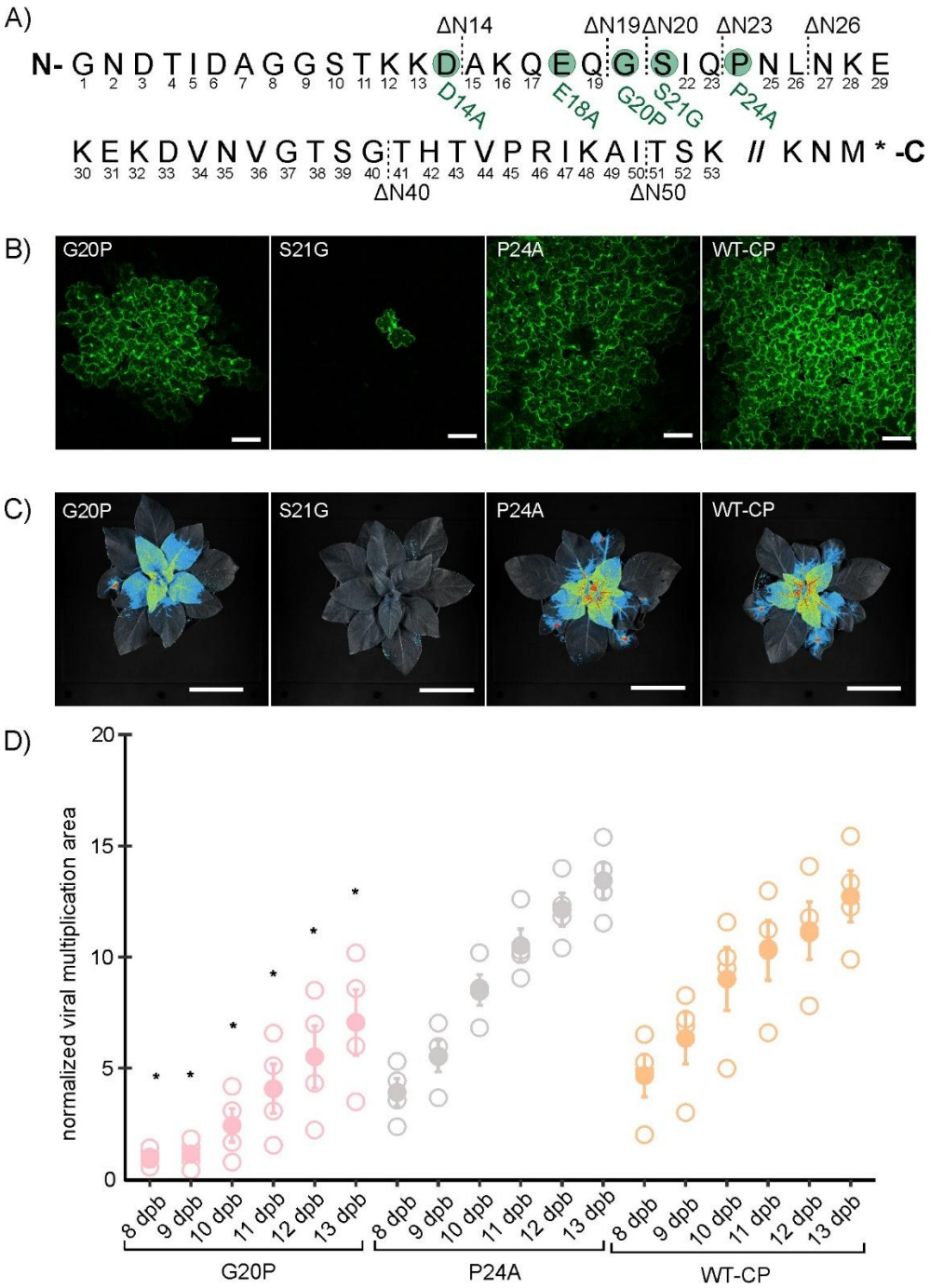

224

225

226 **Figure 4. Substitution of serine to glycine on position 21 of CP N terminal region abolished cell-to-**
227 **cell viral movement and virion assembly. (A)** Amino acid sequence of GFP tagged infectious clone PVY-
228 N605(123) CP protein with labeled constructed deletion and point mutants. The scheme presents mutants
229 with deletions of 14 (ΔN14-CP), 19 (ΔN19-CP), 20 (ΔN20-CP), 23 (ΔN23-CP), 26 (ΔN26-CP), 40 (ΔN40-CP)
230 or 50 (ΔN50-CP) amino acids on CP N terminal region and mutants with point mutations including
231 substitutions of negatively charged aspartic acid to alanine on position 14 (D14A), negatively charged
232 glutamic acid to alanine on position 18 (E18A), glycine to proline on position 20 (G20P), serine to glycine on
233 position 21 (S21G) and proline to alanine on position 24 (P24A). **(B)** Confocal microscopy images showing
234 viral cell-to-cell spread of mutants G20P, S21G, P24A and WT-CP 5 dpb. Scale is 100 µm. **(C)** Spatio-
235 temporal PVY distribution for constructed point mutants G20P, S21G, P24A and WT-CP in *N. clevelandii*
236 systemic tissue as observed by whole plant imaging system 12 dpb. Scale is 5 cm. **(D)** Quantification of viral
237 multiplication area in the upper systemic leaves of bombarded *N. clevelandii* in 6 selected timepoints (8-13
238 dpb). Mean (represented with filled dot) and standard error are shown. Individual measurements are shown
239 as empty dots, representing normalized viral multiplication area. Differences between analyzed point
240 mutants were evaluated with Welch`s t test. Statistically significant differences ($p<0.05$) between G20P
241 mutant and WT-CP are represented with asterisks (*), while there were no statistically observed differences
242 between P24A and WT-CP (see data S8 for all results of statistical testing). Vertical lines present all points
243 except outliers. The results were confirmed in additional experiments (Fig. S5 and data S9).

244 Viral cell-to-cell spread of mutants D14A, E18A and P24A was comparable to WT-CP (Fig. 4B and
245 S6). On the other hand, G20P mutant showed delayed cell-to-cell spread, while S21G mutant
246 remained limited to just single cells at all observed timepoints (Figs. 4B and S6).

247 Next, we performed whole plant imaging to study systemic viral spread of mutants (Figs. 4C and
248 S8). In accordance with the results of cell-to-cell movement, there were no statistically significant
249 differences in viral multiplication area in systemic tissue when comparing D14A, E18A or P24A with
250 WT-CP (Figs. 4D, S7, S5 and data S8, S9, S10, S11) at all observed timepoints. On the other hand,
251 the viral multiplication area of G20P in systemic tissue was statistically significantly lower compared
252 to WT-CP at all observed time points (Fig. 4D and data S8). As expected, S21G did not spread
253 systemically (Fig. 4C).

254 **Discussion**
255
256 The biological function of C and N terminal regions of PVY CP has already been initiated in our
257 previous study, where we hypothesized that N terminal amino acid residues are necessary for an
258 efficient cell-to-cell movement (Kežar et. al., 2019). Here we provide additional insights into the
259 mechanism of PVY spread by identifying the regions of PVY CP N terminal region that are important
260 for efficient viral cell-to-cell movement and systemic infection.

261 Despite the conserved flexible structure of potyviruses N terminal region of CP, there are notable
262 differences observed regarding its involvement in potyviral cell-to-cell and systemic movement. In
263 the case of zucchini yellow mosaic virus (ZYMV), deletion of the entire CP N terminal region did
264 not affect systemic infection (Arazi et. al., 2001). Similarly, a deletion of 6-50 amino acids in the CP
265 N terminal domain did not compromise TuMV cell to cell and systemic movement (Dai et. al., 2020).
266 On the other hand, in tobacco etch potyvirus (TEV), CP N terminal region deletions of 5-29 amino
267 acid residues delayed cell-to-cell movement and prevented systemic spread (Dolja et. al., 1994).
268 We observed inability to move cell-to-cell for PVY when 40 or more amino acid residues were
269 deleted from CP N terminal region (Fig. 1). However, shorter deletions in the range of 19 to 23 did
270 not prevent systemic spread but resulted in delayed systemic and cell-to-cell PVY movement (Figs.
271 2, B and C, 3B and data S4, S3 and S7). The reason behind these observed differences among
272 different potyviral species may be in phylogeny, since ZYMV belongs to bean common mosaic virus
273 (BCMV) supergroup of potyviruses while TEV, PVY and interestingly TuMV as well, to the PVY
274 supergroup (Gibbs and Ohshima, 2010; Gibbs et. al., 2020).

275 The analysis of viral multiplication area revealed important insights into the cell-to-cell movement
276 dynamics of deletion mutants, as increasing number of deleted amino acid residues at CP N
277 terminal region resulted in slower cell-to-cell viral spread (Fig. 2, B and C). Furthermore, slower
278 cell-to-cell virus spread also impacted infection of systemic tissue (Fig. 3A). The connection
279 between cell-to-cell movement and systemic spread was expected, as the virus reaches the veins,
280 enters the veins and is transported in systemic tissue with a delay due to decelerated cell-to-cell
281 movement (Wang, 2015).

282 Results of several studies suggested the role of charged amino acids in the CP core and C terminal
283 region of different potyviruses in cell-to-cell and systemic virus spread (Dai et. al., 2020; Seo et. al.,
284 2013; Tatineni and French, 2014). In contrast, results of our study show that the role of charged
285 amino acids in the CP N terminal region of PVY is not significant, as cell-to-cell spread of D14A
286 and E18A mutants was comparable to WT-CP (Fig. 4B).

287 On the other hand, we observed that replication of S21G mutant was limited to single cells (Fig.
288 4B), which might be due to loss of potential phosphorylation site or disruption of N-terminus
289 structure, due to introduction of glycine. Note that to confirm the hypothesis about the important
290 potential role of phosphorylation of Ser21, we aimed to replace Ser21 also with alanine and
291 threonine, but the design of such point mutants was not achievable, due to their instability in *E. coli*.
292 It has been previously suggested that PVY cDNA is unstable in *E. coli*. Stability of full length PVY
293 plasmids was achieved by inserting introns into putatively toxic genes but still for some mutants
294 recombinations can occur (Bukovinszki et. al., 2007).

295 Furthermore, we also showed the important role of the glycine on position 20 of CP N terminal
296 region in PVY cell-to-cell as well as systemic spread, since G20P mutant spreads slower than WT-
297 CP (Fig. 4 B, C and D). We hypothesize that exchanging Gly with Pro in G20P mutant increased
298 rigidity in the N terminal region. Consequently, the interaction of the CP with other host and viral
299 proteins in the cell may be impaired, resulting in the observed delay. Moreover, alignment of first
300 50 amino acid residues from PVY CP N terminal region across all PVY isolates, revealed a high
301 degree of conservation at the mutated residues between PVY isolates (Fig. S9), further supporting
302 biological significance of our results. The results identifying crucial domains and amino acids of CP
303 N terminal region in viral cell-to-cell movement provided in our study are important basis to
304 elucidate these complex processes, particularly in most economically important viruses such as
305 PVY.

306

307 **Materials and Methods**
308
309 **Plant material**

310 *N. clevelandii* plants were used to follow virus spread. Plants were grown from seeds and kept in
311 growth chambers under controlled conditions as described previously (Baebler et. al., 2009).

312 **Construction of PVY-N605(123)-GFP CP N-terminal deletion and point mutants**

313 As a template to construct mutants with deletions on the CP N terminal region, we used a GFP-
314 tagged infectious clone PVY-N605(123) constructed by Lukan et. al. (2023). The GFP coding
315 sequence was inserted between NIb and CP coding sequences, flanked by protease target
316 sequences, so that GFP would not bother viral movement, since it is excised from the polyprotein
317 as other viral proteins (Lukan et, al., 2023). Megaprimers were designed in accordance with
318 instructions prepared by (Stare et. al., 2020). Detailed information about mutagenic PCR reactions
319 conditions and mixtures can be found in Text S1. After adding 4 µL of DpnI enzyme, the
320 mutagenesis mixtures were transformed into *E. coli* XL 10 Ultracompetent Cells in accordance with
321 manufacturer`s instructions (Agilent Technologies). Transformation mixtures were plated on LB
322 agar with ampicillin selection and incubated overnight at 37ºC. Transformants were screened with
323 colony PCR using PVY GFP_F and PVY uni_R primers (data S12) and KAPA2G Robust HotStart
324 Kit (Agilent Technologies). Prior bombardment, polyprotein and its promoter in PVY-N605(123)
325 lacking 50 and 14 amino acids on CP N-terminus were Sanger sequenced (data S12). Additionally,
326 restriction analysis was performed to confirm the correctness of the PVY coding region.

327 **Biolistic bombardment**

328 Constructed PVY mutants and wild type plasmids were amplified in *E. coli*. Plasmids were then
329 isolated and coated onto gold microcarriers that were used for *N. clevelandii* bombardment using
330 a Helios® gene gun (Bio-Rad), as described by Stare et. al. (2020).

331

332

333 **Plant material sampling and RNA isolation**

334 Plant leaf samples were collected from bombarded *N. clevelandii* plants by excising 0,3 g plant
335 tissue near the bombardment site. Sampled plant material from bombarded *N. clevelandii* leaves
336 was homogenized in 700 µl of RNeasy kit RLT lysis buffer with FastPrep (MP Biomedicals) 1 min
337 6,5 m/s. Total RNA was isolated using RNeasy Plant Mini Kit (Qiagen). Residual DNA was digested
338 with deoxyribonuclease I (DNase I, Qiagen) in solution, using 1.36U DNase/µg RNA. Quality control
339 of isolated RNA was performed as described in Baebler et. al. (2009).

340 **RT-qPCR**

341 Relative PVY RNA concentration was determined by single-step quantitative RT-PCR (RT-qPCR;
342 AgPath-ID One-Step RT-PCR, Thermo FisherScientific) for the ΔN50-CP mutant, while two step
343 RT-qPCR was performed for other mutants. RNA was reverse transcribed with High-Capacity cDNA
344 Reverse Transcription Kit (Thermo Fisher Scientific) and analyzed by qPCR using FastStart
345 Universal Probe Master (Roche).

346 A qPCR assay targeting the PVY CP encoding region was used as a target gene, while the gene
347 encoding for cytochrome oxidase (COX) was used as reference gene. To avoid false positive
348 results plants bombarded with plasmid encoding for blue fluorescent protein, were sampled and
349 analyzed with our qPCR assay targeting PVY CP encoding region. RT-qPCR amplification program
350 and reaction composition mixtures were the same as in Lukan et. al. (2023). Primers and Probes
351 details are listed in data S12.

352 After conducting RT-qPCR reactions, the QuantGenius software (Baebler et. al., 2017) was used
353 for relative quantification of PVY RNA using the standard curve approach. Data containing
354 information about the relative RNA quantity, was averaged for each group and then normalized to
355 the lowest group average number (data S1).

356

357

358 **RT-PCR**

359 One-step reverse transcription PCR (QIAGEN OneStep RT-PCR Kit) was performed to confirm that
360 the introduced mutations were maintained in the viral progeny of all constructed mutants. DNAse-
361 treated RNA, isolated from leaves according to the above protocol, was used as a template.
362 Mutated region was amplified with PVY-GFP_F and uniPVY_R primers (data S12). The purified
363 PCR products were sequenced (Sanger sequencing). For samples with a small amount of mutated
364 virus (ΔN50-CP, ΔN40-CP, S21G), an additional PCR (repliQa HiFi ToughMix; Quantabio) on
365 purified products was performed to amplify the mutated region in sufficient quantity.

366 **Confocal microscopy**

367 Cell-to-cell viral spread on upper side of bombarded *N. clevelandii* leaf discs, sampled with cork
368 borer, was observed under Leica TCS LSI confocal macroscope with Plan APO x5 and x20
369 objectives (Leica Microsystems, Wetzlar, Germany) at different time points (5-14 dpb), and Stellaris
370 5 confocal microscope with HC PL FLUOTAR x10 objective (Leica Microsystems, Wetzlar,
371 Germany) for studying point mutations at 5 dpb. The GFP emission was recorded after excitation
372 with 488 nm laser in the window between 505 and 530 nm and used as a direct measure of the
373 presence of metabolically active viruses in the observed tissue. Sampled discs were scanned
374 unidirectionally with scan speed of 400 Hz and frame average 1 or 2. For following the spread of
375 ΔN50-CP at 12 dpb, 5x and 20x objective were used (Fig. 1B), for ΔN40-CP and WT-CP at 5 and
376 10 dpb, 5x objective was used (Fig. 1B), while for following the spread of ΔN26-CP at 5-14 dpb and
377 ΔN23-CP, ΔN20-CP, ΔN19-CP, ΔN14-CP mutants and WT-CP at 5 dpb, 20x objective was used
378 (Fig. 1C and D). For each mutant we observed at least 3 plants.Images were processed using
379 LEICA LAS X software (Leica microsystems) to obtain maximum projections from z-stacks. Raw
380 confocal microscopy images were deposited at Zenodo (doi: 10.5281/zenodo.16352396).

381 **Virus inoculation**

382 To more precisely examine cell-to-cell viral movement by whole plant imaging, we inoculated 3-4
383 weeks old *N. clevelandii* plants with inoculum prepared from systemic leaves of ΔN14-CP, ΔN19-

384 CP, ΔN23-CP and WT-CP-inoculated plants in which GFP signal was confirmed using whole plant
385 imaging system. Systemic leaves were ground in phosphate buffer (supplemented with PVP 10000)
386 in a plant material : buffer ratio of 1:4. Three bottom leaves of *N. clevelandii* plants were dusted
387 with carborundum powder and rubbed with the inoculum (1-3 drops of inoculum per leaf) which was
388 removed after 10 min by rinsing with tap water.

389 **Whole plant imaging**

390 Cell-to-cell and systemic viral spread throughout the plant was monitored using the Whole plant
391 imaging system Newton 7.0 BIO (Vilber) in bombarded and inoculated *N. clevelandii* plants. GFP
392 emission of GFP-tagged PVY clone was followed in 480 nm excitation channel and emission filter
393 F-550. Images were taken by EvolutionCapt edge software. For viral multiplication area analysis in
394 inoculated leaves, all three ΔN14-CP-, ΔN19-CP-, ΔN23-CP- and WT-CP-inoculated leaves of *N.*
395 *clevelandii* were imaged using exposure time 1 min 46 sec 700 msec, 10x10 field of view (FOV)
396 and 1331-1337 focus in 4 time points: 3 dpi a.m. and p.m. and 4 dpi a.m. and p.m. Measurements
397 for a.m. timepoint were carried out 9 a.m, while for p.m timepoint at 1 p.m. Four plants inoculated
398 with each mutant or WT-CP were imaged. For studying systemic viral spread, at least 3 *N.*
399 *clevelandii* plants bombarded with ΔN26-CP, ΔN23-CP, ΔN14-CP, ΔN19-CP- andWT-CP were
400 imaged, using 50 s exposure time, 20x20 FOV and focus in the range between 1871 and 1905 in
401 different time points (7-12 dpb). Note that *N. clevelandii* plants bombarded with ΔN26-CP and
402 ΔN23-CP were not taken into analysis, due to their inability or big delay in systemic movement. For
403 studying systemic viral spread of point mutations, at least three plants bombarded with constructed
404 point mutants were imaged at different time points (6-13 dpb) with exposure time 50 s and other
405 settings as for studying systemic viral spread of deletion mutants (see above). In case of
406 experiment with D14A and WT-CP at 13 dpb, exposure time was only 5 s to avoid saturation due
407 to a high signal. Raw images were deposited at Zenodo (doi: 10.5281/zenodo.16352396).

408

409

410 **Image analysis and signal quantification following whole plant imaging**

411 Viral multiplication area analysis on inoculated leaves and on upper systemic leaves were
412 performed using Kuant software (Vilber, France). In case of viral multiplication area, surfaces of
413 three viral multiplication areas per leaf were measured, while in case of viral multiplication area in
414 systemic leaves, total count of the virus affected area was measured. Total count is determined as
415 a sum of gray values within region of interest (systemic leaves, ROI) and is proportional to the
416 intensity and spread of the signal. All measured data from Kuant software were exported to Excel,
417 where total count in ROIs were averaged for each timepoint and subsequently normalized on the
418 lowest group average number. Normalized viral multiplication areas were statistically evaluated
419 using Welch`s t-test and were used for graphic representation.

Acknowledgments

We thank Živa Lengar for technical support and laboratory assistance, Dr. Maja Zagorščak and Dr. Angelika Vižintin for help with statistical analysis.

Author contributions

AC, KG and TL designed research; TMP, KS, AC, AV, MTŽ, KB, VL performed the research; AV, TL, TMP, KS, MTŽ, VL, KG, AC, analyzed the data; AV, TL, AC, KG, TMP, KS, MTŽ, IGA, MP, KB, VL contributed to the writing or revision of the article.

Competing interests

The authors declare no competing interests.

Data availability

Raw confocal microscopy and whole plant imaging system pictures were deposited at Zenodo and are openly available at doi: 10.5281/zenodo.16352396).

433 **References**
434

435 Arazi T, Shiboleth YM, Gal-On A. A Nonviral Peptide Can Replace the Entire N Terminus of
436 Zucchini Yellow Mosaic Potyvirus Coat Protein and Permits Viral Systemic Infection. J Virol. 2001;
437 75(14): 6329-6336.

438 Baebler Š, Krečič-Stres H, Rotter A, Kogovšek P, Cankar K, Kok EJ, et al. PVY(NTN) elicits a
439 diverse gene expression response in different potato genotypes in the first 12 h after inoculation.
440 Mol Plant Pathol. 2009; 10(2): 263-275.

441 Baebler Š, Svalina M, Petek M, Stare K, Rotter A, Pompe-Novak M, et al. QuantGenius:
442 Implementation of a decision support system for qPCR-based gene quantification. BMC
443 Bioinformatics. 2017; 18(1): 276.

444 Benitez-Alfonso Y, Faulkner C, Ritzenthaler C, Maule AJ. Plasmodesmata: Gateways to Local
445 and Systemic Virus Infection. MPMI. 2010; 23(11):1403-1412.

446 Bukovinszki A, Götz R, Johansen E, Maiss E, Balázs E. The role of the coat protein region in
447 symptom formation on Physalis floridana varies between PVY strains. Virus Res. 2007; 127: 122-
448 125.

449 Cuesta R, Yuste-Calvo C, Gil-Cartón D, Sánchez F, Ponz F, Valle M. Structure of Turnip mosaic
450 virus and its viral-like particles. Sci Rep. 2019; 9: 15396.

451 Dai Z, He R, Bernards MA, Wang A. The cis-expression of the coat protein of turnip mosaic virus
452 is essential for viral intercellular movement in plants. Mol Plant Pathol. 2020; 21(9):1194-1211.

453 Dolja VV, Haldeman R, Robertson NL, Dougherty WG, Carrington JC. Distinct functions of capsid
454 protein in assembly and movement of tobacco etch potyvirus in plants. EMBO Journal. 1994;
455 13(6):1482-1491.

456 Folimonova SY, Tilsner J. Hitchhikers, highway tolls and roadworks: the interactions of plant
457 viruses with the phloem. Current Opinion in Plant Biology. 2018; 43: 82-88.

458 Gibbs A, Ohshima K. Potyviruses and the digital revolution. Annu Rev Phytopathol. 2010; 48:
459 205-223.

460 Gibbs AJ, Hajizadeh M, Ohshima K, Jones RAC. The potyviruses: An evolutionary synthesis is
461 emerging. Viruses. 2020; 22: 132.

462 Ivanov KI, Eskelin K, Lõhmus A, Mäkinen K. Molecular and cellular mechanisms underlying
463 potyvirus infection. Journal of General Virology. Society for General Microbiology. 2014; 95:
464 1415-1429.

465 Kežar A, Kavčič L, Polák M, Nováček J, Gutiérrez-Aguirre I, Žnidarič MT, et al. Structural basis
466 for the multitasking nature of the potato virus Y coat protein. Sci. Adv. 2019; 5: eaaw3808.

467 Kimalov B, Gal-On A, Stav R, Belausov E, Arazi T. Maintenance of coat protein N-terminal net
468 charge and not primary sequence is essential for Zucchini yellow mosaic virus systemic
469 infectivity. Journal of General Virology. 2004; 85(11): 3421-3430.

470 Kogovšek P, Gow L, Pompe-Novak M, Gruden K, Foster GD, Boonham N, Ravnikar M,
471 Single-step RT real-time PCR for sensitive detection and discrimination of Potato virus Y isolates.
472 J Virol. 2008; 149: 1-11.

473 Lõhmus A, Hafrén A, Mäkinen K. Coat Protein Regulation by CK2, CPIP, HSP70, and CHIP Is
474 Required for Potato Virus A Replication and Coat Protein Accumulation. J Virol. 2017; 91:
475 e01316-16.

476 Lukan T, Županič A, Mahkovec Povalej T, Brunkard JO, Kmetič M, Juteršek M, et al. Chloroplast
477 redox state changes mark cell-to-cell signaling in the hypersensitive response. New Phytologist.
478 2023; 237(2): 548-562.

479 Mäkinen K, Hafrén A. Intracellular coordination of potyviral RNA functions in infection. Vol. 5,
480 Frontiers in Plant Science. Frontiers. 2014; 5: 110.

481 Navarro JA, Sanchez-Navarro JA, Pallas V. Key checkpoints in the movement of plant viruses
482 through the host. In: Advances in Virus Research. 2019; 104: 1-64.

483 Quenouille J, Vassilakos N, Moury B. Potato virus Y: A major crop pathogen that has provided
484 major insights into the evolution of viral pathogenicity. Molecular Plant Pathology. 2013;
485 14(5):439-452.

486 Reagan BC, Burch-Smith TM. Viruses reveal the secrets of plasmodesmal cell biology. Molecular
487 Plant-Microbe Interactions. 2020; 33: 26-39.

488 Revers F, García JA. Molecular biology of potyviruses. Advances in Virus Research. 2015; 92:
489 101-199.

490 Rojas MR, Zerbini FM, Allison RF, Gilbertson RL, Lucas WJ. Capsid Protein and Helper
491 Component-Proteinase Function as Potyvirus Cell-to-Cell Movement Proteins. Vol. 237, Virology.
492 1997; 237: 283-295.

493 Scholthof KBG, Adkins S, Czosnek H, Palukaitis P, Jacquot E, Hohn T, et al. Top 10 plant viruses
494 in molecular plant pathology. Molecular Plant Pathology. 2011; 12: 938-954.

495 Seo JK, Vo Phan MS, Kang SH, Choi HS, Kim KH. The charged residues in the surface-exposed
496 C-terminus of the Soybean mosaic virus coat protein are critical for cell-to-cell movement.
497 Virology. 2013; 446: 95-101.

498 Stare K, Coll A, Gutiérrez-Aguirre I, Žnidarič MT, Ravnikar M, Kežar A, et al. Generation and in
499 Planta Functional Analysis of Potato Virus Y mutants. Bio Protoc. 2020; 10: e3692.

500 Tatineni S, Elowsky C, Graybosch RA. Wheat streak mosaic virus coat protein deletion mutants
501 elicit more severe symptoms than wild-type virus in multiple cereal hosts. Molecular Plant-
502 Microbe Interactions. 2017; 30(12): 974-983.

503 Tatineni S, French R. The C-terminus of Wheat streak mosaic virus coat protein is involved in
504 differential infection of wheat and maize through host-specific long-distance transport. Molecular
505 Plant-Microbe Interactions. 2014; 27(2): 150-152.

506 Tatineni S, Kovacs F, French R. Wheat streak mosaic virus Infects Systemically despite
507 Extensive Coat Protein Deletions: Identification of Virion Assembly and Cell-to-Cell Movement
508 Determinants. J Virol. 2014; 88(2):1366-1380.

509 Wang A. Dissecting the Molecular Network of Virus-Plant Interactions: The Complex Roles of
510 Host Factors. Annual Review of Phytopathology. 2015; 53: 45-66.

511 Wei T, Zhang C, Hong J, Xiong R, Kasschau KD, Zhou X, et al. Formation of complexes at
512 plasmodesmata for potyvirus intercellular movement is mediated by the viral protein P3N-PIPO.
513 PLoS Pathogens. 2010; 6: e1000962.

514 Weller SA, Elphinstone JG, Smith NC, Boonham N, Stead DE, Detection of Ralstonia
515 solanacearum strains with a quantitative, multiplex, real-time, fluorogenic PCR (TaqMan) assay.
516 Appl. Environ. Microbiol. 2000; 66: 2853-2858.

517 Xue M, Arvy N, German-Retana S. The mystery remains: How do potyviruses move within and
518 between cells? Molecular Plant Pathology. 2023; 24: 1560-1574.

519 Yang X, Li Y, Wang A. Research Advances in Potyviruses: From the Laboratory Bench to the
520 Field. Annu. Rev. Phytopathol. 2021; 59: 1-29.

521 Y-W Chung B, Allen Miller W, Atkins JF, Firth AE. An overlapping essential gene in the
522 Potyviridae. Proc. Natl. Acad. Sci. USA. 2008; 105: 5897-5902.

523 Zamora M, Méndez-López E, Agirrezabala X, Cuesta R, Lavín JL, Amelia Sánchez-Pina M, et al.
524 Potyvirus virion structure shows conserved protein fold and RNA binding site in ssRNA viruses.
525 Sci. Adv. 2017; 3: eaao2182.

526

527 **Supporting information captions**

528 **Supplementary Text S1.** Construction of PVY-N605(123)- GFP CP N-terminal mutants
529 **Fig. S1.** ΔN50-CP ΔN40-CP viral replication.
530 **Fig. S2.** Viral replication ΔN26-CP.
531 **Fig. S3.** N19-CP_ΔN14-CP_WT-CP cell-to-cell spread dynamics.
532 **Fig. S4.** ΔN26-CP inability of systemic spread
533 **Fig. S5.** Independent experiment for point mutants G20P, P24A and WT-CP to check viral
534 abundance.
535 **Fig. S6.** Cell-to-cell viral spread of D14A, E18A, G20P, S21G and P24A point mutants.
536 **Fig. S7.** Virus abundance D14A, E18A, WT-CP.
537 **Fig. S8.** Point mutants systemic spread.
538 **Fig. S9.** Alignment of first 50 amino acid residues from the PVY N terminal region across all PVY
539 isolates.
540 **Table S1.** ΔN26-CP viral limitation on single cells or cell-to-cell spread.
541 **Table S2.** Assessed mean intensities of viral fluorescence in ΔN40-CP mutants.
542 **Data S1 (Microsoft Excel format).** Normalized qPCR data for constructed PVY mutants.
543 **Data S2 (Microsoft Excel format).** General sample information including sample name, plant
544 and leaf number, date of putting plants into the soil, date of bombardment.
545 **Data S3 (Microsoft Excel format).** Viral cell-to-cell spread evaluation after *N. clevelandii*
546 inoculation with constructed mutant ΔN23/G-CP and WT-CP.
547 **Data S4 (Microsoft Excel format).** Viral cell-to-cell spread evaluation after *N. clevelandii*
548 inoculation with constructed mutants ΔN19-CP, ΔN14-CP and WT-CP.
549 **Data S5 (Microsoft Excel format).** Viral cell-to-cell spread evaluation after *N. clevelandii*
550 inoculation with constructed mutants ΔN19-CP, ΔN14-CP and WT-CP in replicate experiment.
551 **Data S6 (Microsoft Excel format).** Foci analysis comparisons between experiments.
552 **Data S7 (Microsoft Excel format).** Systemic spread dynamic analysis.
553 **Data S8 (Microsoft Excel format).** Systemic viral spread of G20P and P24A point mutants.
554 **Data S9 (Microsoft Excel format).** Systemic viral spread of G20P and P24A point mutants in
555 replicate experiment.
556 **Data S10 (Microsoft Excel format).** Systemic viral spread of D14A point mutant.
557 **Data S11 (Microsoft Excel format).** Systemic viral spread of E18A point mutant.
558 **Data S12 (Microsoft Excel format).** Primers and megaprimers sequences.
559